Material Testing of Decorative Veneers and Different Approaches for Structural-Mechanical Modelling: Walnut Burl Wood and Multilaminar Wood Veneer

Andreas Dietzel,[a,*] Hendrike Raßbach,[a] and Robert Krichenbauer [b]

A methodology is presented for the determination of elastic material properties on laminated and non-laminated decorative veneers of a variety of wood types. For the uniaxial tensile tests performed, at various temperatures and wood moisture values, the metrological challenges as well as the test results are described and discussed. Subsequently, the characteristic values are transferred into corresponding material models. Also, as the inverse, model-based determination of characteristic values that cannot be determined experimentally is carried out.

Keywords: Veneer; Nonwoven fabric; Composite; Young's moduli; Local and global Poisson's ratios; Tensile test; Out-of-plane deformation; 3D image correlation; Classic laminate theory (CLT); Coupling effects

*Contact information: a: University of Applied Sciences Schmalkalden, Faculty of Mechanical Engineering, Blechhammer, 98574 Schmalkalden, Germany; b: Novem Car Interior Design GmbH, Industriestraße 45, 95519 Vorbach, Germany; *Corresponding author: a.dietzel@hs-sm.de*

INTRODUCTION

Decorative veneers are used in high-quality interior decoration as well as for exclusive interior design in cars and yachts. At the company Novem, the spectrum ranges from very individual, natural veneer, as obtained from burls on the lower section of the trunk, base of the trunk, or the roots of the walnut tree (Buchelt and Wagenführ 2007), to almost freely designable technical veneers. The latter are adapted to their purpose of use through additional production steps. A typical representative of this group is veneer made from multilaminar wood (MLW). This is produced by bonding peeled veneers made from plantation wood (poplar and obeche) to form a solid block of wood in a special process and then slicing it to finished veneer (Castro and Zanuttini 2004). In the industrial environment, this veneer is often known by the brand name ALPI-veneer, after the Italian manufacturer of the same name.

In automobile construction, the use of veneer as a decorative inlay in a variety of mostly three-dimensionally formed plastic parts of the interior has become established. For this, if necessary, the veneers are provided with a stabilising lamination material, usually preformed, and then back-injected in an injection moulding tool. Apart from this, an optically transparent protective coating, also plastic, is applied to the visible side. The manufacture of such components consequently requires the correct design of a variety of tools as well as the adjustment of the necessary process parameters.

For the design of injection moulds, with respect to rheological filling, tool cooling, as well as shrinkage and warping of the finished component, today numerical simulation is implemented as the standard tool (Brinkmann 2010; Kennedy and Zheng 2013). In

contrast, for the forming of veneer, in most cases empirical values are used (Buchelt and Wagenführ 2007; Bellair 2012).

Now if, as described, veneer forming and the injection moulding process are combined, then the design of suitable tools and processes is costly and involves a great deal of time. Here, suitable simulation models could provide a remedy.

Firstly 3 cases of application can be defined for these models:

1. Preforming of the veneers
2. Interaction of veneer and inflowing polymer melt in the injection moulding process; here at the same time the veneer is greatly stressed both mechanically and thermally
3. Influence of the veneer on the warping behaviour of the plastic product as it cools and is demoulded from the tool

In addition, veneers are often stabilised with textile laminates on the back side before further processing. To also be able to investigate these influences with the help of simulation calculations in the product development process, suitable structure-mechanical characteristic values of decorative veneers and laminating material are indispensable.

Wood, due to its structure, as well as the combinations of veneer and lamination material can be included in the material group of functionally graded materials (FGM). This material group is gaining in importance, so that in this area mechanical modeling is also driven forward (Belabed *et al.* 2014; Hebali *et al.* 2014). Thus the presented methodology is also of interest for materials from the designated area, in addition to the veneer-processing industry for many other industries.

EXPERIMENTAL

Material

The purpose of the present investigations was the derivation of a suitable methodology for the determination of the characteristic values of thin (0.3 mm) decorative veneers with and without lamination, with the objective of direct transfer into structure-mechanical material or simulation models.

The description of the material behaviour of thin layers of wood (veneers) cannot be carried out with characteristic values obtained from solid wood. The reason for this is primarily the manufacture-related changes or damage to the structure, such as cracks during slicing or peeling the veneers (Buchelt and Pfriem 2011; Pfriem and Buchelt 2011; Bellair 2012; Dupleix *et al.* 2013).

For this reason, the investigations were carried out directly on veneers. A natural veneer made from walnut burl wood and a technical veneer made from MLW of the version ALPI-fineline were tested. In addition, a laminating material as well as a material composite made from veneer and laminate were investigated. Table 1 provides an overview of the tested materials.

Table 1. Tested Materials

Index	Material	Specification	Thickness (mm)
M01	veneer, sliced	walnut burl wood (natural veneer)	0.37
M02	Veneer, sliced	MLW-ALPI fineline (technical veneer)	0.38
M03	textile	nonwoven fabric[1], 90 g*m^{-2}	0.25
M04[2]	composite	faced on backside with M03	0.46
[1] wet-laid, nonwoven, long fibred fabric: pulp-fibres solidified with polyester-fibres and water-based binders [2] strain measurement on front side (veneer surface)			

Objective

With respect to the cases of model application defined for veneer forming and injection moulding process (see Introduction), first, all characteristic values that are necessary for a linear-elastic material description according to Hooke (Eq. 1) are derived for the veneers under investigation.

$$\{\varepsilon\} = [\mathrm{D}] * \{\sigma\} \; ; \; \{\sigma\} = [\mathrm{C}] * \{\varepsilon\} \; ; \; \mathrm{C} = \mathrm{D}^{-1} \tag{1}$$

The description of the material behaviour for wood is usually based on three different, growth-related directions (Eq. 2).

$$\begin{aligned} 1 &\coloneqq \mathrm{L} \quad \parallel \text{ to fibre} \quad \text{(longitudinal)} \\ 2 &:= \mathrm{R} \quad \perp \text{to fibre} \quad \text{(radial)} \\ 3 &:= \mathrm{T} \quad \perp \text{to fibre} \quad \text{(tangential)} \end{aligned} \tag{2}$$

If the material flexibility tensor $[\mathrm{D}]$ is formulated in these three main material directions, Hooke's law is produced as shown in Eq. 3.

$$\begin{Bmatrix} \varepsilon_{11} \\ \varepsilon_{22} \\ \varepsilon_{33} \\ \gamma_{12} \\ \gamma_{23} \\ \gamma_{31} \end{Bmatrix} = \begin{bmatrix} \frac{1}{\mathrm{E}_{11}} & -\frac{\nu_{21}}{\mathrm{E}_{22}} & -\frac{\nu_{31}}{\mathrm{E}_{33}} & 0 & 0 & 0 \\ -\frac{\nu_{12}}{\mathrm{E}_{11}} & \frac{1}{\mathrm{E}_{22}} & -\frac{\nu_{32}}{\mathrm{E}_{33}} & 0 & 0 & 0 \\ -\frac{\nu_{13}}{\mathrm{E}_{11}} & -\frac{\nu_{23}}{\mathrm{E}_{22}} & \frac{1}{\mathrm{E}_{33}} & 0 & 0 & 0 \\ 0 & 0 & 0 & \frac{1}{\mathrm{G}_{12}} & 0 & 0 \\ 0 & 0 & 0 & 0 & \frac{1}{\mathrm{G}_{23}} & 0 \\ 0 & 0 & 0 & 0 & 0 & \frac{1}{\mathrm{G}_{31}} \end{bmatrix} \begin{Bmatrix} \sigma_{11} \\ \sigma_{22} \\ \sigma_{33} \\ \tau_{12} \\ \tau_{23} \\ \tau_{31} \end{Bmatrix} \tag{3}$$

Because it is handled differently in the literature, Eq. 4 shows the indexing of the Poisson's ratios used here. These are defined as the ratio of the strains perpendicular to the load direction ε_{jj} and in the load direction ε_{ii} .

$$\nu_{ij} = -\frac{\varepsilon_{jj}}{\varepsilon_{ii}} \; ; \; i,j = 1,2,3 \; ; \; i \neq j \tag{4}$$

For numerical solution approaches, it is usually required that the material flexibility tensor $[\mathrm{D}]$ be symmetrical. For this reason, the following symmetry conditions (Eq. 5) are to be established for orthotropic materials.

$$\frac{\nu_{12}}{E_{11}} = \frac{\nu_{21}}{E_{22}} \;;\; \frac{\nu_{13}}{E_{11}} = \frac{\nu_{31}}{E_{33}} \;;\; \frac{\nu_{23}}{E_{22}} = \frac{\nu_{32}}{E_{33}} \tag{5}$$

In addition, because of the manufacturing process (slicing), it is to be assumed for the investigated veneers that the veneer plane comprises mixed forms of the main material planes 12 (LT) and 13 (LR). Consequently, because these planes cannot be differentiated explicitly in the test, the simplification of the material description to a transverse-isotropic model is meaningful and necessary. This describes only the two preferential directions parallel (∥) and perpendicular (⊥) to the fibre. Because of the isotropy assumption, in the plane perpendicular to the fibre, the equivalences according to Eq. 6 are produced, whereas Eq. 7 describes the shear modulus in this plane (Mang and Hofstetter 2008). The shear modulus $G_{\parallel\perp}$ can be calculated with the correlation (Eq. 8) discovered by Lekhnitskij (Lekhnitskij 1981; Bellair *et al*. 2012),

$$\begin{array}{lllll} E_{11} & & & = & E_{\parallel} \\ E_{22} & = & E_{33} & = & E_{\perp} \\ G_{12} & = & G_{31} & = & G_{\parallel\perp} \\ G_{23} & & & = & G_{\perp\perp} \\ \nu_{12} & = & \nu_{13} & = & \nu_{\parallel\perp} \\ \nu_{23} & = & \nu_{32} & = & \nu_{\perp\perp} \end{array} \tag{6}$$

$$G_{\perp\perp} = \frac{E_{\perp}}{2(1+\nu_{\perp\perp})} \tag{7}$$

$$G_{\parallel\perp} = \frac{E_{\parallel} * E_{\perp}}{E_{\parallel} + E_{\perp} + \nu_{\perp\parallel} * E_{\parallel} + \nu_{\parallel\perp} * E_{\perp}} \tag{8}$$

The number of material parameters to be determined, which is **12** according to Eq. 3, is consequently reduced to **4** with the aid of Eqs. 5 to 8.

Test Methodology

The determination of the characteristic values was carried out with the help of uniaxial tensile tests. To take into account the anisotropic properties of the materials, the two main material directions, parallel (∥) and perpendicular (⊥) to the fibre, were tested.

Furthermore, with solid wood as well as veneer, the great dependency of the characteristic values of stiffness and strength on wood moisture and temperature is known (Fuchs 1963; Bellair 2012; Ozyhar *et al*. 2013). To determine the bandwidth of the influence of the characteristic values here, four different test climates were realised as key values; see table 2.

For the tests, a Zwick universal testing machine (Zwick GmbH & Co. KG, Ulm, Germany) was used, which was equipped with a climatic chamber (climates P1, P3) or a special test module (climates P4, P5) (Bellair 2012). The measurement of the strain took place over the entire surface, optically in the parallel part of the test specimen (measuring field: 30 mm x 10 mm), using the 3D digital image correlation (DIC) measuring system Aramis2M (GOM - Gesellschaft für Optische Messtechnik mbH, Braunschweig, Germany). Through direct coupling with the testing machine and our own software expansions, a synchronous recording of data and semi-automated characteristic value extraction (Dietzel *et al*. 2010) was realised. The use of full-surface 3D deformation-/strain measurement makes it possible to detect and evaluate effects like material inhomogeneities and out-of-plane deformations. For the materials to be examined such effects are expected

(Bellair 2012; Buchelt and Wagenführ 2007). In contrast to the aforementioned studies, in this work explicitly the impact of these effects on derivation of material parameters and a consistent material parameter set is investigated.

The derivation of the elastic characteristic values (moduli of elasticity–MOE's, Poisson's ratios) was carried out by means of a regression calculation at a uniform strain-based interval per series, (*e.g.*, $[\,0.2, 0.9\,] * \varepsilon_{max}$) of the stress-strain- or lateral strain-longitudinal strain curves (series = combination of material, test climate, fibre orientation). This interval was defined such that the linear range of the curves was covered as completely as possible. The evaluation interval of material M03 (textile) was matched to the interval of the significantly stiffer and more brittle material M02 (MLW-veneer). The aim was to derive a linear-elastic material description of the multilayer material M04 (composite), valid until failure of the veneer. Suitable test speeds were determined in preliminary tests based on the standards DIN 52188 (1979) and DIN 52377 (1978). To be able to compare the results of all tested materials, possible speed-dependent influences were kept constant by defining a uniform test speed of 1 mm min^{-1}.

As specimen shape, according to Bellair (2012), the dumbbell specimen based on DIN 52377 (1978) was selected at a scale of 1:2. All materials listed in Table 1 were ground to a target thickness of 0.3 mm (the material composite to 0.5 mm), so that in each case, uniform layers of wood approximately 0.3 mm thick were produced. Cutting to size was then carried out using a laser. With material M01 (walnut burl wood), despite the natural, heavy graining of this type of wood, it was attempted during the sample preparation to fashion the sampling from the veneer, so that at least the strain measuring field (middle of the sample) is oriented to the main material directions parallel (∥) or perpendicular (⊥) to the fibre.

Table 2. Test Climates

Index	Temperature	Relative humidity	Test envi-ronment	Moisture content	Comment
-	T (°C)	RH (%)	-	w [%]	-
P1	20	65	climatic chamber	12	Reference (normal climate wood/plywood, DIN 52188/DIN 52377)
P3	120	-	climatic chamber	0	maximum test temperature (see purpose of tests, section introduction)
P4	20	-	test module	FS	maximum amount of water absorption (in the cell walls)
P5	70	-	test module	FS	P4 superimposed with temperature (metrological compromise)
FS - above fibre saturation; tested in water (cell walls filled to maximum, additional free water in the lumen, $w = w_{max}$)					

To reinforce the veneer at the clamping points, force application elements made from 5 mm beech wood were glued on at both sides. Finally, a stochastic grayscale pattern, necessary for the optical strain measurement, was applied in the spray process. From this stochastic pattern a point cloud of the sample surface is calculated by the image processing

software for each loading condition. The local displacements of these points are used to calculate deformation and strain vectors. The exact test cross-section of all individual samples was measured, after storage in the laboratory for approximately one week (approximately 23 °C/50% relative humidity (RH)), with a Vernier calliper (width) and an outside micrometer gage (thickness). The mean values are specified in Table 1. Before the test, the samples were preconditioned for at least 48 h in their respective test climates.

Because of the large number of influencing parameters to be investigated, a sample size of 5 was defined for each test series. This resulted in a total sample size of 160. Because of the low sample size for each series, an extraction of statistical key figures was not considered expedient. Therefore, for each series, from the measured values of the individual samples, only the median value $\tilde{x}$ as well as the smallest and largest measured value were determined as criterion for the spread width. For reasons of comparability, the characteristic values are shown normalised to the respective series characteristic value for fibre-parallel (∥) testing under standard climate P1 (20 °C/65% RH).

RESULTS

Walnut Burl Wood Veneer (M01, Natural Veneer)

Failure behaviour

The typical different fracture patterns (splintered fibre fracture, cleavage fracture), depending on the load direction, as known with other deciduous wood veneers (Winter 1955; Bellair 2012), could not be determined. The failure occurred almost always in the parallel part of the test specimen, with the crack path approximately perpendicular to the load direction, but thereby following typical macroscopic structure features. Figure 1 shows to what extent macroscopic structure features (grain), local differences in strain, and crack path correlate.

Specific effects

Depending on the wood structure (grain), the full surface strain measurement already allows great, local differences in the strain behaviour of the material to be detected. For the evaluation of the Poisson's ratios, this fact is also taken into account. Figure 1 illustrates to what extent these differ locally in the recorded measurement field. Deviations from the mean value $\bar{\varepsilon}$ of the strain in this field are shown, such as in the range $[\, 0 \leq \bar{\varepsilon} \leq 2\bar{\varepsilon} \,]$.

The phenomenon was found to be even more acute with samples that had been tested at moisture contents above fibre saturation (FS: P4, P5). Here, local deviations up to $[\, -2\bar{\varepsilon} \leq \bar{\varepsilon} \leq 4\bar{\varepsilon} \,]$ were measured, which means a change in polarity sign, *i.e.*, contracting and expanding zones in the lateral direction, depending on the position in the measurement field.

A correlation with the wood structure was verified. It was shown that zones with extreme longitudinal strains did not correlate with zones of extreme lateral strains.

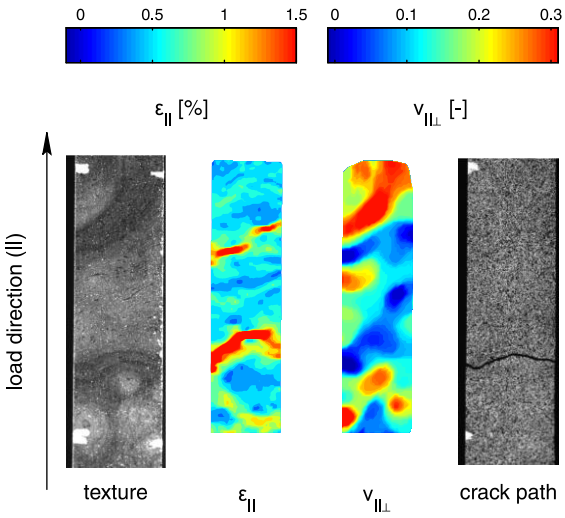

Fig. 1. M01 (walnut burl wood veneer), strain measurements at maximum load, P1 (20 °C/65% RH): wood structure (sample without grayscale pattern) / strain in load direction $\boldsymbol{\varepsilon}_{\parallel}$ / local Poisson's ratios $\boldsymbol{\nu}_{\parallel\perp}$ / crack path (sample with grayscale pattern)

Elastic properties

The measurement results did not indicate any considerable directional dependency (∥, ⊥) of the determined moduli of elasticity and Poisson's ratios (Fig. 2).

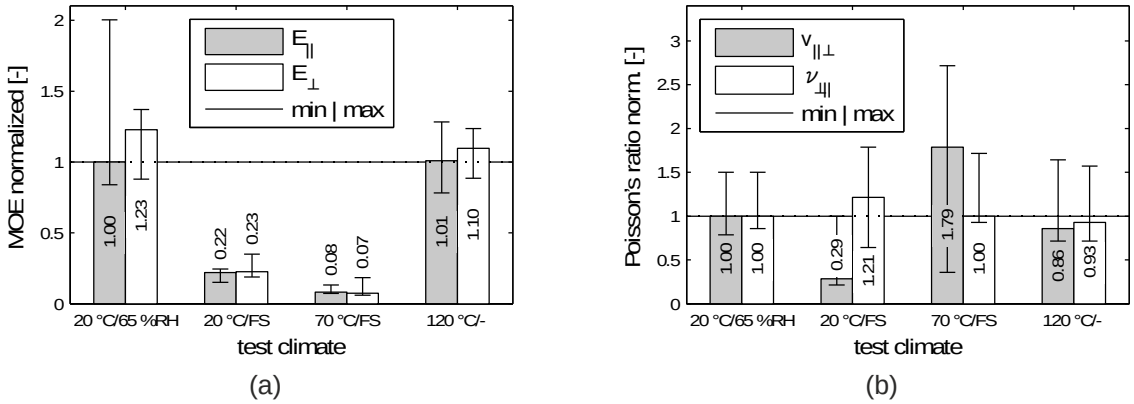

Fig. 2. M01 (walnut burl wood veneer), measuring results normalised: (a) moduli of elasticity $\tilde{\mathbf{E}}$ and (b) Poisson's ratios $\tilde{\boldsymbol{\nu}}$

For the measured MOEs (Fig. 2a), the dependency on wood moisture and temperature turned out to be very obvious. In contrast, major differences in the Poisson's ratios (Fig. 2b) dependent on the test climate were not identifiable.

The spread width of the measured values in every series turned out to be quite large. Large local differences of the lateral strain-/longitudinal strain ratio in the strain measurement field could be determined as a major influencing factor for this.

Evaluation

The present results suggest that a growth-related, global directional dependency of the material properties, as with solid wood, does not exist for walnut burl wood veneer. The application of a global, orthotropic material model, as described, cannot be

recommended. The use of an isotropic material model must be validated with the help of the determined, greatly climate-dependent MOEs of the material. The extent to which simulation models thereby developed are able to supply helpful results for the fields of application defined must be tested with real component geometries (see Introduction, cases of application: 1. Preforming of veneers, 2. Interaction of veneer and inflowing polymer melt in the injection moulding process, 3. Influence of the veneer on the warping behaviour of the plastic product while cooling and demoulding).

Multilaminar Wood Veneer (M02, Technical Veneer)

Failure behaviour

The samples loaded in the fibre direction featured a splintered fibre fracture. The tendency to split was considerable more pronounced on the samples tested above the fibre saturation humidity.

Specific effects

The manufacture of dumbbell samples from material M02 (MLW) with a fibre load angle of 90° proved to be not realisable. The very low strength of the material perpendicular (⊥) to the fibre made non-destructive handling impossible. Consequently, no samples could be tested perpendicular to the fibre.

For the evaluation of the series P4 (20 °C/FS) and P5 (70 °C/FS), the determined Poisson's ratios first showed implausible values. In particular, a negative polarity sign or a change of polarity sign was noticeable as the sample load was increased.

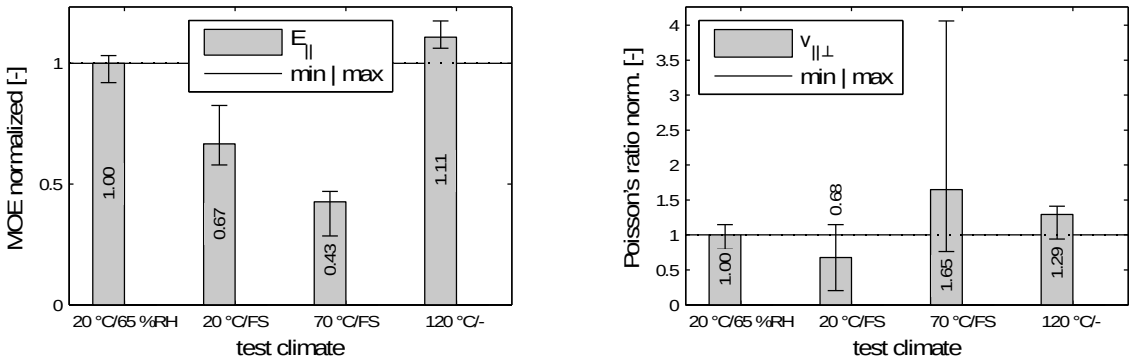

Fig. 3. M02 (multilaminar wood veneer), measuring results normalised: (a) moduli of elasticity $\tilde{\mathbf{E}}$ and (b) Poisson's ratios $\tilde{\boldsymbol{\nu}}$

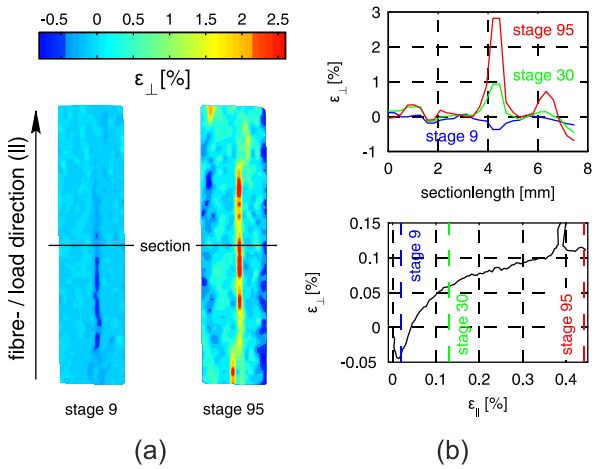

Fig. 4. M02 (multilaminar wood veneer), P4 (20 °C/FS), strains lateral to the load direction ($\boldsymbol{\varepsilon}_{\perp}$): (a) contour plot of 2 load states (b) above: $\boldsymbol{\varepsilon}_{\perp} = \mathbf{f}(\mathbf{sectionlength})$ / below, mean values of measuring field: $\boldsymbol{\varepsilon}_{\perp} = \mathbf{f}(\bar{\boldsymbol{\varepsilon}}_{\parallel})$

A detailed evaluation revealed cracks in the sample in longitudinal direction, which at the time were already present in the unloaded state. These cracks were closing or opening through load transfer effects during the tensile test. That makes an evaluation of a mean lateral strain on the entire surface impossible, as these local effects, which are recorded metrologically as quasi-strains (crack opening/-closing), overlay the lower basic lateral strains of the material. For the reasons mentioned, for series P4, only two samples could be used for the calculation of a Poisson's ratio; with series P5, there were only three.

Whether these cracks can be traced back to water-retention effects (*e.g.*, swelling, failure of the MLW-adhesive bonds) is unclear. However, it can be determined that these only occurred with series P4 and P5 (above fibre saturation). Figure 4 shows an example, based on a test specimen of series P4 (20 °C/FS), of how these crack movements are shown over various load stages and are reflected in the strain curve.

If a cut is made straight through the test specimen and applied above the lateral strain (Fig. 4b, above), the local strain superelevation at the crack can be seen very clearly.

Figure 4b (below) shows the development of the lateral strain $\varepsilon_{\perp}$ as the load increases, *i.e.*, increasing strain $\varepsilon_{\parallel}$ in load direction. The perpendicular lines show the cut, for several stages, in the curve shape, which represents values averaged over the measuring surface.

For the interpretation of Fig. 4:

1. Stage 9, at the beginning of the tensile test: local strong contraction (dark blue - existing, gaping crack closes)
2. Stage 30, following on: reversal to positive lateral strain
3. Stage 95, shortly before the end of the tensile test: marked positive strain measured value (red – crack opens)

Elastic properties

The measured MOEs (Fig. 3a) indicate a strong dependency on the wood moisture and the temperature, as do the Poisson's ratios (Fig. 3b). The Poisson's ratios of the series

P4 (20 °C/FS) and P5 (70 °C/FS) are only conditionally meaningful for the reasons mentioned (cracks) and should therefore be assessed critically.

Evaluation

The results indicate the dependency of the elastic material properties on temperature and humidity. As shown, with respect to the determination of the characteristic values, the technical veneer made from MLW involved considerable difficulties. Experiences with tensile test samples of other, natural veneers suggest that, in particular, the combination of differently stiff layers of wood and adhesive present in MLW-veneer increases the fragility. Whether geometric modifications of the test specimens, in size and material thickness, could provide a remedy here must, if necessary, be investigated more closely. Because these veneers are only used in laminated form by the Novem company, the additional effort does not seem to be justified at present.

Wet-Laid Nonwoven (M03, Textile)

Failure behaviour

The investigated textile had a clearly recognisable texture. Regardless of their orientation (∥, ⊥) the test specimens featured a greatly deformed cleavage fracture. This occurred uniformly in the parallel part of the dumbbell test specimen. Such cracks ran approximately perpendicular (⊥) to the load direction. In contrast to the series P1 (20 °C/65% RH) and P3 (120 °C), test specimens that had been tested in climates P4 (20 °C/FS) and P5 (70 °C/FS) featured a clear local necking in the area of the fracture.

Specific effects

Because of very high elongations of fracture of the material, strains until fracture could not be recorded for all tests. The reason lies in the principle of the optical measuring system, which, with test specimens that are too greatly deformed (to greatly changed surface grayscale pattern), no longer permits any correlation to the non-deformed state.

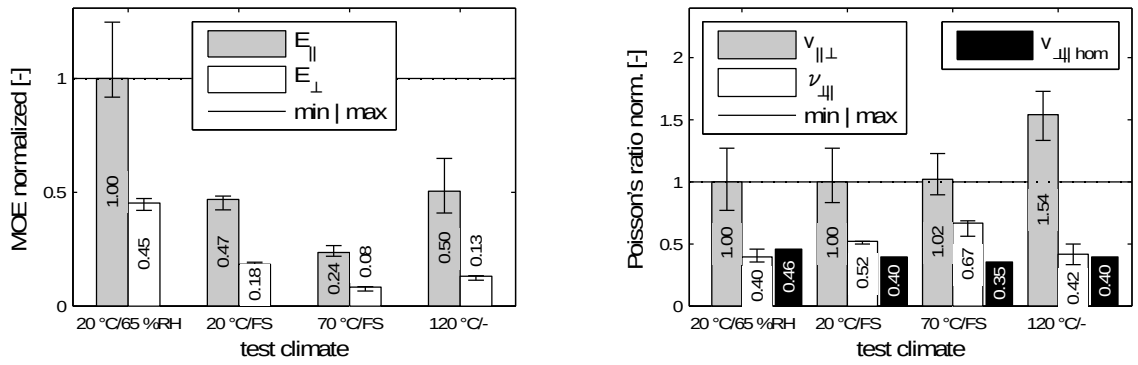

Fig. 5. M03 (textile), measuring results normalised: (a) moduli of elasticity $\tilde{\mathbf{E}}$ and (b) Poisson's ratios $\tilde{\boldsymbol{\nu}}$

Elastic properties

The measured MOEs (Fig. 5a) showed considerable differences with increased humidity or temperature, whereas the determined Poisson's ratios (Fig. 5b) exhibited only

slight dependencies. Only with an increase in temperature to 120 °C was an increase in the Poisson's ratio to approximately 150% indicated in the texture direction (fibre direction).

Evaluation

For the textile used as laminating material, an orthotropic material modelling could be applied. The characteristic values necessary for this could be extracted from the present tests.

The characteristic values determined in the tensile tests performed here are mathematically processed values. These are median values of every test specimen series, which only immediately satisfy the symmetry conditions (Eq. 5) in the rarest of cases. To ensure the symmetry of the flexibility tensor, various homogenisation strategies can be applied (Bellair 2012). In the following, the adaptation of the smaller Poisson's ratio is implemented, *i.e.*, this characteristic value is calculated with the help of the converted symmetry condition (Eq. 9).

$$\nu_{\perp\parallel\,\mathrm{hom}} = \frac{E_{\perp}}{E_{\parallel}}\nu_{\parallel\perp} \tag{9}$$

The results of the homogenisation $\nu_{\perp\parallel\,\mathrm{hom}}$ are also specified in Fig. 5b.

Composite Material (M04, MLW | Textile)

Failure behaviour

The test specimens loaded in the fibre direction featured a cleavage fracture that ran more or less perpendicular (⊥) to the load direction. The fracture path thereby differed evident from the splintered fibre fracture with non-laminated veneer. Here, the laminating material obviously demonstrated its stabilising effect. In test climate P5 (70 °C/FS), this was displayed as slightly weakened, and the tendency to splinter was again clearly visible. The climate-related greatly reduced stiffnesses and tensile strengths of the laminating material could be responsible for this.

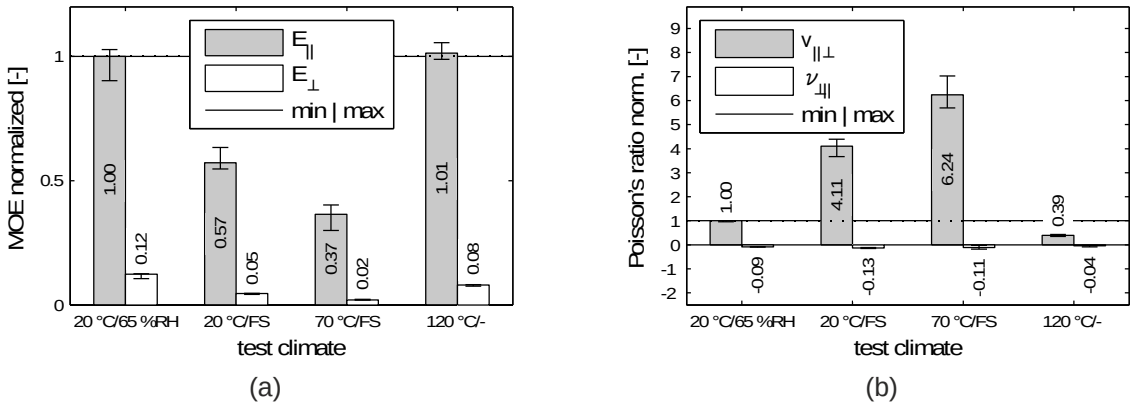

Fig. 6. M04 (composite), measuring results normalised: (a) moduli of elasticity $\tilde{\mathbf{E}}$ and (b) Poisson's ratios $\tilde{\boldsymbol{\nu}}$

Specific effects

The evaluation of the measurement results revealed that the tested material composite, consisting of two orthotropic individual layers, featured obvious effects, which are known in the case of asymmetrically layered fibre composite materials and can be

described, *e.g.*, with the help of classic laminate theory (CLT; Moser 1992). Essentially, these are as follows:

1. Bending-Strain-Coupling
   - in all climates
   - when tested perpendicular (⊥) to fibre
   - hardly/not verifiable with test parallel (∥) to fibre

2. Curvature from changes in moisture content
   - in climates P4 (20 °C/FS) and P5 (70 °C/FS)
   - on samples oriented parallel (∥) to fibre

Elastic properties

The measured MOEs (Fig. 6a) indicate a similar great dependency on wood moisture and temperature as the basic materials of the multilayer composite. The stiffnesses parallel (∥) and perpendicular (⊥) to the fibre had a ratio of approximately 10:1 for all climates.

Poisson's ratios were calculated from the strains measured in lateral and loading direction for all test climates and material orientations (Fig. 6b). However, because of the effects mentioned, these can only be applied for test specimens tested parallel (∥) to the fibre for climates P1 (20 °C/65% RH) and P3 (120 °C) in the sense of the material constant $\nu_{\parallel\perp}$. The comparison of these two values reveals a considerable temperature dependency (Fig. 6b).

Evaluation

To understand the observed, metrological phenomena resulting from the tested material composite, their causes should be briefly described more closely:

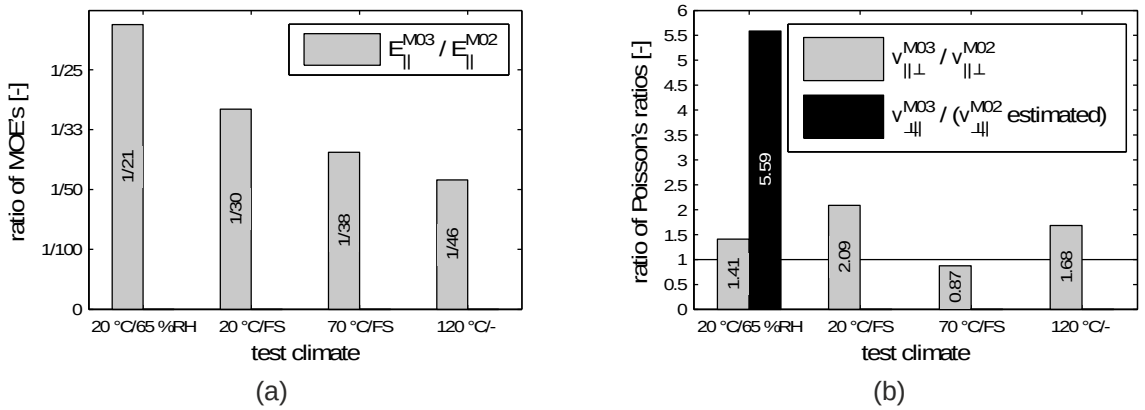

Fig. 7. Ratios of ply materials M03/M02 (Textile/MLW): (a) MOE's $\tilde{\mathbf{E}}$ and (b) Poisson's ratios $\tilde{\boldsymbol{\nu}}$; $\boldsymbol{\nu}_{\perp\parallel}^{\mathbf{M02}}$ estimated based on common ratios of deciduous wood and standard climate $\boldsymbol{\nu}_{\perp\parallel}/\boldsymbol{\nu}_{\parallel\perp} \approx \mathbf{1/10}$ (Bellair 2012; Ozyhar *et al.* 2013)

1. Bending-Strain-Coupling (all test climates):
   The Poisson's ratios of all test specimens loaded perpendicular (⊥) to the fibre first featured implausible values in the form of a negative polarity sign. The detailed analysis revealed a curvature effect (Fig. 8) during increasing tensile loading as the cause.

The relevant effects:

(a) The veneer and the textile lamination featured greatly different Poisson's ratios $\nu_{\perp\parallel}$ (Fig. 7b) and moduli of elasticity $E_{\parallel}$ (Fig. 7a) lateral to the loading direction

Example, Climate P1 (20 °C/65% RH)

$$\frac{\nu_{\perp\parallel\,\text{textile}}}{\nu_{\perp\parallel\,\text{veneer}}} \approx 5 \;;\; \frac{E_{\parallel\,\text{textile}}}{E_{\parallel\,\text{veneer}}} \approx \frac{1}{20}$$

(b) The asymmetric elongation in the lateral direction (∥) occurring under tensile loading (⊥) subsequently led to a curvature *h* of the test specimen over its longitudinal axis. At maximum load this curvature *h* was about 0.05 to 0.1 mm, for the test specimen width *w* of 10 mm (Fig. 8).

(c) This bending effect did not result in any compression in the lateral direction; rather, there was an elongation of the non-laminated test specimen surface.

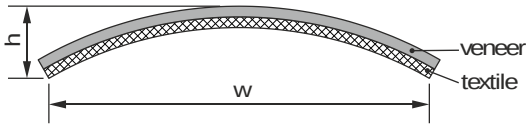

Fig. 8. Curvature about the longitudinal axis of the specimen (width x height)

2. Curvature from changes in moisture content:

During the analysis of the test specimens loaded parallel (∥) to the fibre with climate settings P4 (20 °C/FS) and P5 (70 °C/FS), the globally determined Poisson's ratios initially indicated the correct sign of polarity, but very high values, which must be regarded as implausible (numerical values: 2 ... 3). After detailed analysis of the 3D deformation measurements, here a curvature of the test specimen over its longitudinal axis, that was already present in the non-loaded state, proved to be responsible.

The relevant effects:

(a) The veneer swelled, mostly lateral to the fibre (Niemz 1993), because of water retention (preconditioning). The back side textile did not swell or swelled clearly less.

(b) The inhibited asymmetric elongation subsequently led to a curvature *h* of the test specimen of about 0.5 to 1 mm, relative to the test specimen width *w* of 10 mm (Fig. 8).

(c) Because of the forced flatness of the test specimen in the clamping area, under tensile load the curvature existing in the middle of the test specimen (measuring field) went back ("pulling smooth").

(d) A compression (negative elongation) of the non-laminated test specimen surface resulted from this bending effect.

The measured lateral strain is therefore an overlay of the specified bending effect (curvature goes back) and actual lateral strains of the material composite. The Poisson's ratio derived from this is therefore not meaningful in the sense of a material constant and is greatly dependent on the existing swell ratios and the forced boundary conditions resulting from the clamping.

Modelling of the Composite Material M04

To conclude to what extent the model approaches presented in combination with the determined characteristic values can be applied to describe the deformation behaviour of laminated veneers, various model calculations were performed. Thereby, the effects determined in the uniaxial tensile test should be forecast by the model. For this, it was restricted to the results of the climate P1 (20 °C/65% RH).

Model 1, Virtual Substitute Material

For the evaluation of the thesis, that the veneer-textile composite can be regarded as a virtual substitute material, a simple mixture rule (Eq. 10) was applied.

$$E_{i,composite} = E_{i,veneer}\frac{t_{veneer}}{t} + E_{i,textile}\frac{t_{textile}}{t} \;\; ; \;\; i = 1,2\ (\parallel,\perp) \qquad (10)$$

The stiffnesses of the present individual components (veneer, textile) were thereby grouped to a resulting stiffness $E_{i,composite}$ according to their proportions on the test cross section (width(w) x thickness(t)) of the tensile test specimen. The spring model in Fig. 9 visualises the basic idea of this mixture rule. For the reasons mentioned, this model could only be applied for characteristic values parallel (∥) to the fibre. In comparison with the measured results, the resulting model error was close to 25% (Table 3).

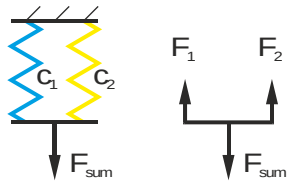

Fig. 9. Rule of mixture

The main cause for this deviation is inadequate knowledge of the ply thicknesses of veneer and lamination. To illustrate: an error in the measurement of 0.01 mm means, relative to the ply thickness (≈ 0.2 mm), a deviation in thickness of 5%. It was previously assumed that Eq. 11 applies, *i.e.*, the veneer thickness t_{veneer} can be calculated from the measured material thicknesses of the composite and the textile (Experimental section; get target thickness of the composite by grinding process).

$$t_{\text{veneer}} = t_{\text{composite}} - t_{\text{textile}} \quad (11)$$

However, measurements of the ply thicknesses in the microscope (Fig. 10) show that the textile lamination was compacted through application on the veneers, consequently producing a deviating veneer thickness $t_{veneer;\,corr}$. The consideration of this corrected thickness led to a reduction of the model error to 19% (Table 3). Figure 10 also shows the major error that this improved method of thickness determination reveals, with a boundary layer veneer/textile that can only be defined exactly with great difficulty.

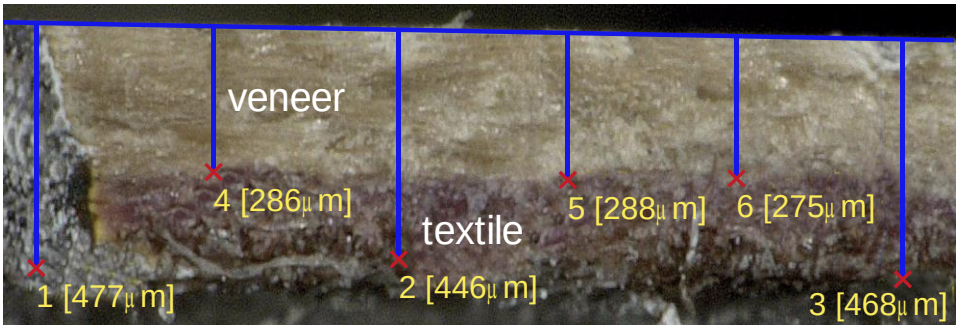

Fig. 10. Thicknesses of plies M04 (composite)

The compacting of the textile lamination is not investigated in more detail here, as it is assumed that the stiffness properties are not influenced by this or only to a very slight extent. In other words, it is still calculated based on the cross-section values and area-related characteristic values known from the testing of the pure textile (M03).

Model 2, FEM Layered Shell

Because the remaining model error still turned out to be relatively high, a second calculation model of the tensile test specimen was developed. For this, the following approaches were implemented, known from CLT.

For the description of the individual layer, CLT makes use of the simplification of the plain stress state (Moser 1992). With that, Hooke's law (Eq. 3) for orthotropic materials switches to a reduced form (Eq. 12). The stress- $\{\sigma\}$ and strain- $\{\varepsilon\}$ vectors each contain only three elements; the material stiffness matrix $[C]$ is therefore transferred to the reduced stiffness matrix $[Q]$. A single ply is regarded as a two-dimensional structure and described with the help of the mechanical model of the shell. The area-related values are transformed into values normalised to the shell width. These are related to the mid-plane of the structure and therefore, in addition to the strain, also require consideration of the shell curvature $\{\kappa\}$ (Eq. 13). For layered materials, these internal forces are then summed up over all individual plies *k* (Eqs. 14 and 15), usually obtained at the mid-plane ($z = 0$) of the composite, and as a result describe its deformation behaviour (Eq. 16).

$$\{\sigma\} = \{\sigma_{\parallel} \quad \sigma_{\perp} \quad \tau_{\parallel\perp}\}^{T} = [Q] * \{\varepsilon\} \quad (12)$$

$$\{\sigma\} = [Q] * [\{\varepsilon\} + \{\kappa\}] \quad (13)$$

$$\{n\} = \sum_{k=1}^{n} [Q]_k * \left[\int_{z_{k-1}}^{z_k} \{\varepsilon^0\}\, dz + \int_{z_{k-1}}^{z_k} \{\kappa\}\, z\, dz \right] \quad (14)$$

$$\{m\} = \sum_{k=1}^{n} [Q]_k * \left[\int_{z_{k-1}}^{z_k} \{\varepsilon^0\}\, z\, dz + \int_{z_{k-1}}^{z_k} \{\kappa\}\, z^2\, dz \right] \quad (15)$$

$$\begin{Bmatrix} n \\ m \end{Bmatrix} = \begin{bmatrix} A & B \\ B & D \end{bmatrix} * \begin{Bmatrix} \varepsilon^0 \\ \kappa \end{Bmatrix} \quad (16)$$

It can be seen from (Eq. 16) that, in addition to extensional- $[A]$ and bending- $[D]$, now coupling stiffnesses $[B]$ also exists in the model, through which the effect of bending-extension-coupling observed with the material composite (M04, MLW | Textile) can be mapped.

The calculation model was performed as a finite element model (Fig. 11) in ANSYS with the help of layered shell elements (shell281). As a result, the layer structure and exact boundary conditions from the test specimen geometry and clamping are considered in the calculation. The comparability with the stress-strain behaviour recorded in the test was ensured as follows:

- Strains
  - equivalent to the recording with ARAMIS, *i.e.*, averaged over the strain measurement field
  - calculated at the TOP side of layer 2 (Fig. 11)
- Stresses
  - calculated engineering stresses (ratio of reaction forces to test specimen cross-section)

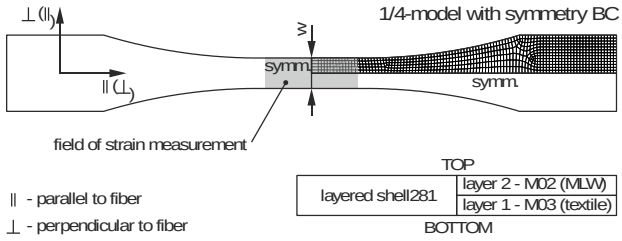

Fig. 11. FE model, M04 (composite)

In addition to the pure recalculation of the uniaxial tensile test, parameter studies were also carried out to inversely determine the characteristic values modulus of elasticity $E_\perp$ and Poisson's ratio $\nu_{\perp\parallel}$ of the veneer that could not be determined in the test. Thereby, in addition to the measurement data for single plies and the composite, its measured curvature was also used as a reference while loading the test specimen perpendicular (⊥) to the fibre. As a result, the following model error remained for the composite:

- elastic characteristic values ≤ 11% (Table 3)
- curvature $h \approx$ 50% (Fig. 12)

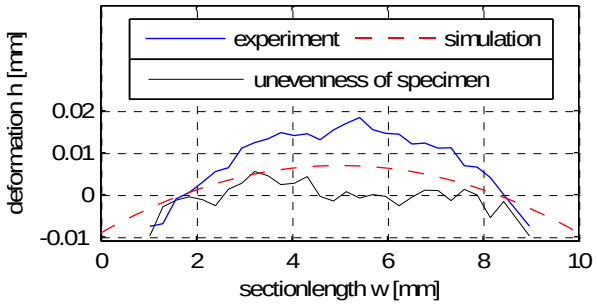

Fig. 12. Curvature of M04 (composite) at max. load, P1 (20 °C/65% RH), load perpendicular (⊥) to the fibre

With respect to Fig. 3, the inversely determined characteristic values of the MLW-veneer (M02) were:

$$\frac{E_{\perp}}{E_{\parallel}} = \frac{\nu_{\perp\parallel}}{\nu_{\parallel\perp}} = \frac{1}{8.5}$$

It should be noted that the negative Poisson's ratio of the composite $\nu_{\perp\parallel}^{M04}$ measured in the test is difficult to recreate in the model (positive strain in lateral direction from overlayed curvature, Fig. 6b). The curvature (Fig. 12) is always represented, whereas the negative polarity signs could only be achieved through a massive reduction of the effect-relevant Poisson's ratio of the veneer $\nu_{\perp\parallel}^{M02}$ by at least a factor of 10.

Whether this can be traced back to prior damage to the MLW-veneer (cracks; see Fig. 4), the basic unevenness of the real material not taken into account in the model (Fig. 12), or another effect in connection with the model error of the curvature, leaves room for further investigation.

Table 3. Elastic Properties of Composite (M04), Models in Relation to Measurement

Models			Elastic properties		
			$E_{\parallel}$	$E_{\perp}$	$\nu_{\perp\parallel}$
(measurement = 100%)			(%)	(%)	(%)
1.1	Virtual material		75	-	-
1.2	Virtual material ($t_{veneer;\,corr}$)		81	-	-
2	FEM, layered shell		89	96	(80)

CONCLUSIONS

1. To summarise, it can be stated that the description of the structure-mechanical behaviour of decorative veneers is relatively complex. Here, an orthotropic material model description, as is common for wood, cannot automatically be regarded as the method of choice.

2. By means of examples based on two typical, decorative veneers used in industry (walnut burl wood-, multilaminar wood veneers), the results presented point out their essential differences in the material behaviour. The differences when using laminating materials were demonstrated by means of an example of a nonwoven textile used in the industry. The derived characteristic values quantified the great dependency on temperature and moisture content, both with veneer as well as laminating material.
3. The use of a full-surface, 3D recording image correlation system for the measurement of the deformations/ strains proved to be very advantageous. Major effects that could be traced back to local differences in the material behaviour as well as out-of-plane deformation could only be determined this way and interpreted for the purpose of a material model description.
4. At the same time, the metrological peculiarities of the testing of material composites consisting of veneer and laminating material in a uniaxial tensile test were highlighted. The different moisture expansion behaviour, the great differences at moduli of elasticity, and Poisson's ratios, as well as the determination of the thickness of the individual plies stood out as the major sources of error. For these reasons, testing of the respective ply materials is to be favoured and if necessary supplemented with tests of the composite. Ideally, these composite tests should be carried out in parallel to model calculations to be able to record, interpret, and map relevant effects.
5. The modelling of the material composite also requires special attention and cannot be recommended in the form of a "smudged" approach, which does not explicitly resolve the individual plies. In contrast, the application of more essential approaches of classic laminate theory (CLT), commonly used to describe layered fibre-composite materials, turned out to be suitable. With the help of an analytical and a finite element model (layered shell elements), the uniaxial tensile test was recreated and aligned with the test results. The model error could be minimised; as a result, the FE-model could also be used for the inverse determination of characteristic values that cannot be determined in the tensile tests.
6. With respect to the different complexity of the cases of application of simulation calculations defined under section introduction, further investigations are necessary. In particular, the description of the material failure must be expanded further, *i.e.*, suitable failure criteria must first be defined. Effects such as the local failure of the veneer layer (local crack opening of a few $1/100$ mm) do not initially represent any defect from a production-related perspective, but they must be taken into consideration in the calculation model in a suitable way. Here, a continuum mechanical description of the ply materials in the form of elasto-plastic-(orthotropic) material models holds great potential.

REFERENCES CITED

Belabed, Z., Houari, M. S. A., Tounsi, A., Mahmoud, S. R. and Anwar Bég, O. (2014). "An efficient and simple higher order shear and normal deformation theory for functionally graded material (FGM) plates," *Composites: Part B* 60, 274–283. DOI:10.1016/j.compositesb.2013.12.057

Bellair, B. (2012). *Beschreibungb des anisotropen Materialverhaltens von Rotbuchenfurnier als Basis für rechnergestützte Umformsimulationen*, PhD thesis, Faculty of Mechanical Engineering, Technische Universität Ilmenau, Ilmenau, Germany

Bellair, B., Dietzel, A., Zimmermann, M., Raßbach, H., and Zimmermann, K. (2012). "A contribution to the description of the mechanical behaviour of veneer using a linear elastic orthotropic material model," *Problems of Mechanics* 49(4), 11-21.

Brinkmann, T. (2010). *Handbuch Produktentwicklung mit Kunststoffen*, Hanser Verlag, Munich, Germany.

Buchelt, B., and Pfriem, A. (2011). "Influence of wood specimen thickness on its mechanical properties by tensile testing: Solid wood versus veneer," *Holzforschung* 65(2), 249-252, DOI: 10.1515/HF.2011.032

Buchelt, B., and Wagenführ, A. (2007). "Untersuchungen zur Anisotropie der mechanischen Eigenschaften von Nussbaummaserfurnier (*Juglans nigra L.*)," *European Journal of Wood and Wood Products* 65(5), 407-409. DOI: 10.1007/s00107-007-0172-x

Castro, G., and Zanuttini, R. (2004) "Multilaminar wood: Manufacturing process and main physical-mechanical properties," *Forest Products Journal* 54(2), 61-67.

Dietzel, A., Bellair, B., Zimmermann, M., and Raßbach, H. (2010). "Universelle optische Dehnungsmesstechnik für Serienprüfungen der Materialkennwertermittlung, Datenaufbereitung und Prozessüberwachung," in: Der Rektor (ed.), Proceedings, University of Applied Sciences Schmalkalden, Schmalkalden, Germany, 11. Nachwuchswissenschaftlerkonferenz, pp. 323-326.

DIN 52188 (1979). "Testing of wood; Determination of ultimate tensile stress parallel to grain," German Institute for Standardization (DIN), Berlin, Germany.

DIN 52377 (1978). "Testing of plywood, determination of modulus of elasticity in tension and of tensile strength," German Institute for Standardization (DIN), Berlin, Germany.

Dupleix, A., Denaud, L. E., Bleron, L., Marchal, R., and Hughes, M. (2013). "The effect of log heating temperature on the peeling process and veneer quality: Beech, birch, and spruce case studies," *European Journal of Wood and Wood Products* 71(2), 163-171. DOI: 10.1007/s00107-012-0656-1

Fuchs, F. R. (1963). *Untersuchungen über den Einfluss von Temperatur und Holzfeuchtigkeit auf die elastischen und plastischen Formänderungen von Buchenholz bei Zug- und Druckbelastung*, PhD thesis, Universität Hamburg, Hamburg, Germany

Hebali, H., Tounsi, A., Houari, M.S.A., Bessaim, A. and Adda Bedia, E.A. (2014). "New quasi-3D hyperbolic shear deformation theory for the static and free vibration analysis of functionally graded plates," *Journal of Engineering Mechanics* 140(2), 374–383. DOI:10.1061/(ASCE)EM.1943-7889.0000665

Kennedy, P., and Zheng, R. (2013). *Flow Analysis of Injection Molds*, 2nd ed., Hanser Verlag, Munich, Germany.

Lekhnitskij, S. G. (1981). *Theory of Elasticity of an Anisotropic Body*, Mir-Publisher, Moscow, Russia.

Mang, H., and Hofstetter, G. (2008). *Festigkeitslehre*, 3rd Ed., Springer-Verlag, Vienna, Austria.

Moser, K. (1992). *Faser-Kunststoff-Verbund*, VDI-Verlag, Düsseldorf, Germany.

Niemz, P. (1993). *Physik des Holzes und der Holzwerkstoffe. Holz : Anatomie-Chemie-Physik*, DRW-Verlag, Leinfelden-Echterdingen, Germany.

Ozyhar, T., Hering, S., and Niemz, P. (2013). "Moisture-dependent orthotropic tension compression asymmetry of wood," *Holzforschung* 67(4), 395-404. DOI: 10.1515/hf-2012-0089

Pfriem, A., and Buchelt, B. (2011). "Influence of the slicing technique on mechanical properties of the produced veneer," *European Journal of Wood and Wood Products* 69(1), 93-99. DOI: 10.1007/s00107-010-0410-5

Winter, H. (1955). "Unterlagen und Richtlinien für den Holzflugzeugbau: B III b Sperrhölzer," Technical Report, Technische Hochschule Braunschweig, Braunschweig, Germany.

Article submitted: April 12, 2015; Peer review completed: June 26, 2016; Revisions accepted: July 1, 2016; Published: July 18, 2016.
DOI: 10.15376/biores.11.3.7431-7450